PHILOSOPHICAL TRANSACTIONS OF THE ROYAL SOCIETY A MATHEMATICAL, PHYSICAL & ENGINEERING SCIENCES

Tunnelling in Thin SiO$_{2}$

D. R. Wolters and A. T. A. Zegers-Van Duijnhoven

Phil. Trans. R. Soc. Lond. A 1996 **354**, 2327-2350
doi: 10.1098/rsta.1996.0103

Tunnelling in thin SiO_2

By D. R. Wolters and A. T. A. Zegers-van Duijnhoven
Philips Research Laboratories, 5656 AA Eindhoven, The Netherlands

The conduction of electrons through ultra-thin insulators is accurately described by the Fowler–Nordheim mechanism. Electrons tunnel through the energy barrier at the cathode interface to the conduction band of the insulator and drift to the anode. The mechanism is the same as for field emission from cold cathodes in vacuum.

In very thin oxides of 30–80 Å, tunnelling is modulated by quantum-interference effects. Injected electrons form standing waves in the oxide conduction band interfering with their tunnelling probability. These quantum oscillations enable the determination of layer thicknesses to a high precision.

Accompanying the tunnelling current, a 'substrate-hole current' is often observed by carrier separation techniques, but its origin is still in debate. We have now conducted experiments for several oxide layers between 30 and 70 Å in which we show that the substrate-hole current coherently follows the quantum oscillations of the tunnel current. This new fact rules out the earlier explanations based on anode-hole tunnelling and valence-band electron tunnelling.

Injection of electrons in wide band-gap dielectrics is by no means harmless. The energy loss of the electrons, especially at the anode interface, leads to degradation of the properties of the dielectric. This explains the generation of mesoscopic features, or 'trees', extending over several atomic distances. The formation of the 'trees' is modelled by computer simulation. The degradation of the dielectric leads to increased current leakage, negative or positive space-charge evolution and dielectric losses. Persisting charge transport renders strongly degraded insulators and finally causes dielectric breakdown.

Nomenclature

A	cm^2	capacitor area
$\mathrm{Ai}[z]$		Airy function
$\mathrm{Ai}'[z]$		derivative of $\mathrm{Ai}[z]$
$\mathrm{Bi}[z]$		Airy function
$\mathrm{Bi}'[z]$		derivative of $\mathrm{Bi}[z]$
C	$\mathrm{F\ cm}^{-2}$	capacitance per unit area
d	cm	oxide thickness
E	J	energy
E_{disp}	$\mathrm{J\ cm}^{-2}$	displacement energy stored per cm^2 of the capacitor
E_{F}	J	Fermi energy
$\mathcal{E}$	$\mathrm{V\ cm}^{-1}$	electric field
$\mathcal{E}_{\mathrm{bd}}$	$\mathrm{V\ cm}^{-1}$	value of $\mathcal{E}$ at breakdown
F		cumulative probability of breakdown
G	S	conductance
h	J s	Planck's constant
$\hbar$	J s	$h/2\pi$

Phil. Trans. R. Soc. Lond. A (1996) **354**, 2327–2350
Printed in Great Britain

I	A	current
J	A cm^{-2}	current density
J_{FN}	A cm^{-2}	Fowler–Nordheim current density
$J_{\max}$	A cm^{-2}	current density at infinite field, supply current density.
k	J K^{-1}	Boltzman constant
k_{an}	cm^{-1}	electron wave number in anode
k_{cat}	cm^{-1}	electron wave number in cathode
k_{ox}	cm^{-1}	electron wave number in oxide conduction band
m	kg	electron mass in empty space
m_{an}	kg	electron mass in anode
m_{ox}	kg	electron mass in oxide conduction band
m_{cat}	kg	electron mass in cathode
N	eV^{-1}cm^{-3}	electron density
Q	C cm^{-2}	charge fluence flowing through the capacitor
Q_{bd}	C cm^{-2}	charge fluence leading to breakdown for a capacitor
t	s	time
t_{ox}	cm	length of electron path in conduction band
$\mathcal{T}$	J	kinetic energy
T	K	temperature
V	V	voltage applied to the capacitor
v	cm s^{-1}	velocity of electron
x_{l}	cm	distance in oxide conduction band
x_{t}	cm	tunnel distance
β	V cm^{-1}	characteristic field for Fowler–Nordheim injection
Φ	eV	potential energy
Φ_{b}	eV	effective barrier height
ϵ_{ox}	F cm^{-1}	dielectric constant of the oxide
λ	cm	characteristic damping length
λ_{abs}	cm	characteristic absorption length
ω	rad s^{-1}	frequency

1. Introduction

The injection of electrons through dielectrics is used in memories, like electrical (erasable) programmable read only memories (E(E)PROMS), to store information for longer time. Unintentional injection occurs in metal oxide silicon (MOS) devices, especially with thin dielectrics (less than 100 Å) and operated with more than 5 V on the gate. In both cases, the injection produces degradation and breakdown shortening the operational lifetime of the microcircuit. Therefore, research is needed on the mechanism of charge transport and degradation.

Electronic charge transport through thin silica films on silicon is best described by the so-called Fowler–Nordheim conduction (Fowler & Nordheim 1928). The mechanism consists of quantum mechanical tunnelling of electrons through the energy barrier at the cathode–insulator interface. It is similar to the field emission of electrons from cold cathodes into a vacuum (Van Oostrom 1965). Lenzlinger & Snow (1969) were the first to explain the current–voltage curves of capacitors of thermally grown SiO_2 by the Fowler–Nordheim mechanism. Weinberg (1977) investigated tunnelling in unmetallized SiO_2 layers on silicon, measuring the decay of the surface potential with a Kelvin probe.

Maserjian (1988) was the first to show that in very thin oxides, of less than 80 Å the Fowler–Nordheim curve is modulated by an extra field-dependent factor. They assigned this to quantum-interference effects. Side-effects of tunnelling are light emis-

sion and substrate currents assigned to the generation of holes. Eitan & Kolodny (1983) modelled the hole currents in the substrate, related to the tunnelling electron current. They attributed this to electron tunnelling from the valence band of the silicon into the conduction band of the oxide. Each tunnelling electron leaves a hole in the valence band. Weinberg & Fisschetti (1985), however, showed this explanation to be inconsistent with intercepts and slopes of the Fowler–Nordheim curves. The mechanism is still under debate. Numerous measurements on conduction and breakdown are given in the references.

In this paper we shall give a short overview of published results and present some new results which shine a new light on the substrate hole current. Furthermore we shall review earlier work on degradation and breakdown which is the eventual result of continued tunnelling. After a short introduction of the Fowler–Nordheim field emission equation, we shall discuss the general shape of barrier transmission probability and supply current. Temperature, image force, band bending and surface structure effects will be briefly indicated. For very thin dielectrics quantum-interference effects or 'quantum oscillations' superposed on the Fowler–Nordheim plot are shown. Our results are compared with published work.

Side effects of field emission are substrate-hole currents and light emission. The occurence of quantum oscillations in the substrate-hole currents is new, as we have recently observed. The fact that these oscillations in the substrate-hole currents are coherent with the Fowler–Nordheim current rebuts all existing models. We hope this will contribute to new insight in the matter.

Other side-effects of field emission currents are the irreversible change of properties and degradation leading to breakdown. Computer modelling of this degradation and breakdown will be presented. We show that for modern ultrathin oxides the Q_{bd} model for breakdown, as developed for thicker oxides, still applies.

2. Field emission in dielectrics

The Fowler–Nordheim equation can be applied to the tunnelling mechanism of electrons through thin oxide layers, as shown by Lenzlinger & Snow (1969). To apply the formal equation we must, however, be aware of the differences between tunnelling in thin oxides and tunnelling in vacuum. In contrast to vacuum emission, electrons in thin oxides can return to their original position, e.g. by reflection from the anode. The ratio of the change in wavelength of the electron $\Delta\lambda/\Delta x$ in the oxide and the distance between anode and cathode, d, is the critical parameter. The characteristic length for energy loss is about 6 Å, as we shall see below. The semi-classical approach is valid when the layer thickness is roughly above 80–100 Å. We will make a distinction between classical and wave-mechanical effects by first treating relatively thick oxides (greater than 100 Å) and then thin oxides (less than 80Å). However, first we will discuss the general form of field emission as used for cold cathodes in vacuum.

(*a*) *Field emission in general*

The formal expression for field emission of electrons by a cold cathode in vacuum is given by the Fowler–Nordheim equation in concise form by:

$$J_{\mathrm{FN}} = J_{\max}\mathrm{e}^{-\beta/\mathcal{E}}, \tag{2.1}$$

where J_{FN} is the current density in A cm^{-2}, $\mathcal{E}$ is the oxide field at the injecting electrode in MV cm^{-1}, $\mathrm{e}^{-\beta/\mathcal{E}}$ is the probability of passing through a barrier by field

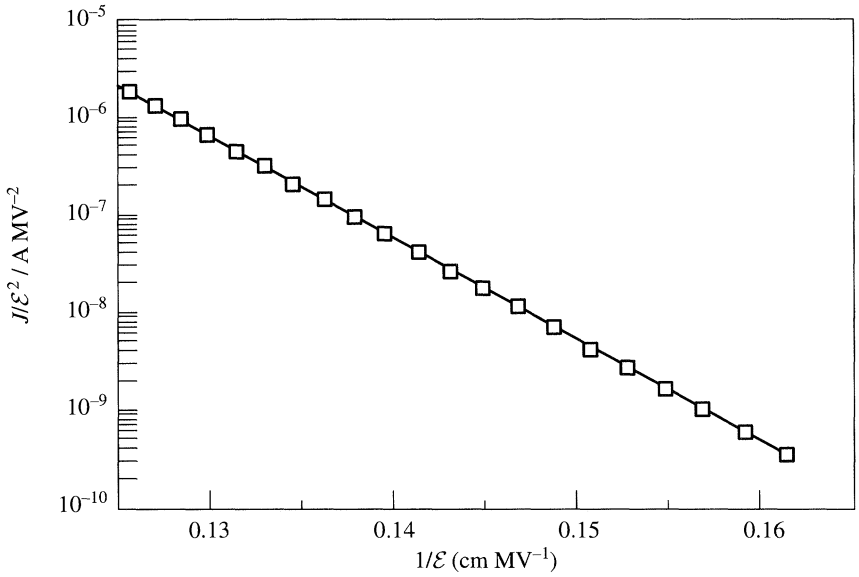

Figure 1. Fowler–Nordheim plot of current through an MOS-capacitor. 11.3 nm oxide, gate = n^+ poly, area 6×10^{-3} cm^{-2}.

emission, and $J_{\max}$ is the total number of electrons multiplied by the number of trials per second per cm^2 (Weinberg 1982):

$$J_{\max} = \frac{q^3 m \mathcal{E}^2}{16\pi^2 \hbar m_{\mathrm{ox}} \Phi_{\mathrm{b}}} \tag{2.2}$$

and

$$\beta = \frac{4}{3} \frac{\sqrt{2m_{\mathrm{ox}}}}{q\hbar} \Phi_{\mathrm{b}}^{3/2}, \tag{2.3}$$

where q is the electron charge, m is the mass of the electron in empty space, m_{ox} is the mass of the electron in the oxide, $2\pi\hbar$ is Planck's constant and Φ_{b} is the effective barrier energy in electronvolts.

When investigating minor variations of the tunnelling probability with the field strength, $\mathcal{E}$, e.g. for quantum oscillations, it is convenient to rearrange equation (2.1) to

$$\beta(\mathcal{E}) = \mathcal{E} \ln \frac{J_{\max}}{J_{\mathrm{FN}}} \quad (\mathrm{MV\ cm^{-1}}). \tag{2.4}$$

Least squares fitting of the Fowler–Nordheim plot yields accurate values of $J_{\max}$, and then values of $\beta(\mathcal{E})$ can be calculated accurately. An example of a Fowler–Nordheim plot is shown in figure 1. A straight line can be fitted to the data by least squares regression techniques. The regression coefficient is 99.9% which shows that the Fowler–Nordheim equation fits in an excellent way to the measurements. The barrier height for this capacitor is calculated to be $\Phi_{\mathrm{b}} = 2.91$ eV which is close to other values reported in literature (Weinberg 1982).

(*b*) *Field emission in thick oxide layers*

The best known derivation of the Fowler–Nordheim equation is semiclassical. The derivation assumes large momenta and tunnelling distances and potential fields with

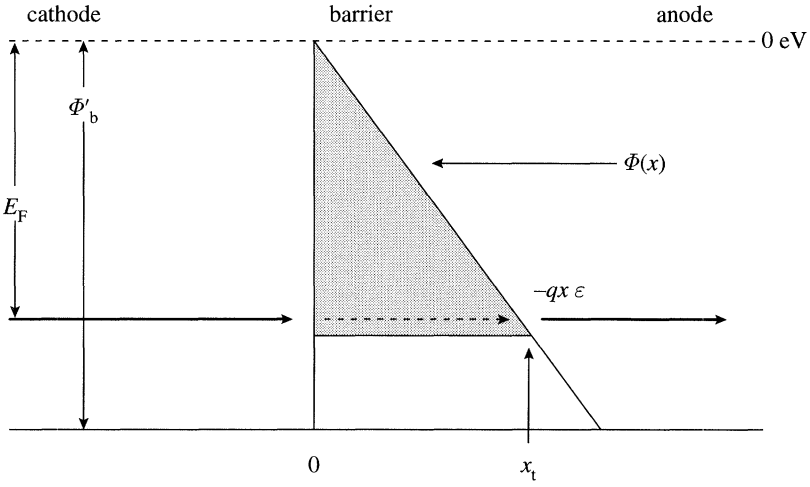

Figure 2. Tunnelling through a triangular barrier.

small gradients in order to use the WKB approximation. For sharply rising potential barriers at low temperatures, as we have in the case of the abrupt transition at a silicon–oxide interface, the condition of large momenta and of smooth potential gradients is not really fulfilled. Still, the approximation gives an excellent description for thick dielectrics. The tunnelling mechanism through a triangular barrier is depicted in figure 2. The total energy of the electron in the x-direction is given by

$$E = \mathcal{T}(x) + \Phi(x), \tag{2.5}$$

where $\mathcal{T}(x)$ is the kinetic energy in the x-direction and $\Phi(x)$ the potential energy. To reach the other side of the barrier the electron needs to borrow an amount of action

$$\int_0^{x_t} \sqrt{2m_{ox}|\Phi'_b - \Phi(x) - E|}\,\mathrm{d}x,$$

where x_t is the tunnel distance through the barrier. The more action that is heeded, the less probable the tunnelling process will be. Assuming a triangular barrier we can replace $|\Phi'_b - \Phi(x) - E|$ by $|E - q\mathcal{E}x|$, where $\mathcal{E}$ is the field. Φ'_b is the barrier height measured to the bottom of the conduction band.

$$\text{Prob} \approx \exp\left[-\frac{2}{\hbar}\int_0^{x_t}\sqrt{2m_{ox}|E - q\mathcal{E}x|}\,\mathrm{d}x\right] \approx \exp\left[-\frac{4}{3}\frac{\sqrt{2m_{ox}}}{\hbar q\mathcal{E}x}|E|^{3/2}\right]. \tag{2.6}$$

In metal cathodes we can replace E by Φ'_b. In silicon the barrier height Φ'_b differs from E by band bending effects, as we shall see below.

Implicit assumptions are the triangular barrier, a smooth surface, a temperature of 0 K and free-electron approximation in cathode and anode.

(i) *Factors affecting the barrier height*

The theoretical transition probability for triangular barriers underestimates experimental currents, mainly due to five effects, to be discussed below.

Temperature. The main effect of temperature is that a number of electrons can pass the barrier from a level higher than the lowest level. Practically all the electrons which can pass the barrier originate from levels in the high energy tail of the Fermi

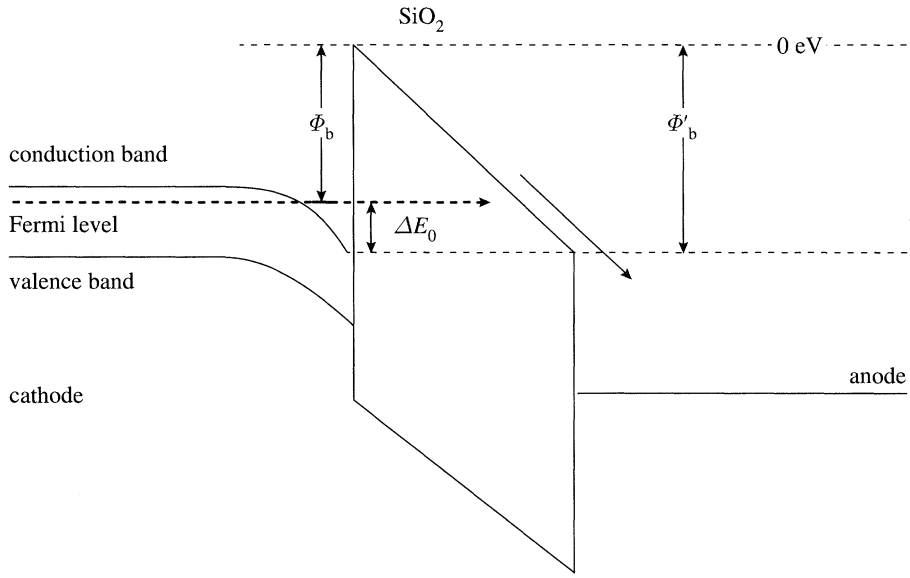

Figure 3. Tunnelling in an MOS capacitor from a subband E_0.

distribution (Van Oostrom 1965). The relative increase of the current is given by the dependence of the pre-exponential factor:

$$\frac{\Delta J}{J} \propto \frac{T^2 \Phi_b^2}{\mathcal{E}^2}, \tag{2.7}$$

which is about the reciprocal of the pre-exponential term. Therefore the temperature predominantly affects the current at low fields.

Band-bending effect. If there is pronounced band bending, the electrons cannot be confined to the bottom of the conduction band due to the uncertainty principle. The effect is that electrons must occupy levels at an energy E_0 higher than the conduction band edge. This reduces the effective height to $\Phi_b = \Phi'_b - \Delta E_0$, as depicted in figure 3. ΔE_0 is of the order of 0.3 eV for severe band bending in silicon (Weinberg 1982).

The image-force effect. The electron at the cathode is attracted by its image. Therefore its potential energy increases rapidly with distance from the cathode. The image-force energy tends to lower the barrier energy. Under our experimental conditions this lowering of the potential barrier is not noticeable, however (Weinberg 1982).The image force effect would show up as a curvature in the Fowler–Nordheim plot, which is seldomly observed. Linear regression shows that the curvature is so small at operational fields that for silicon oxide layers the effect can be neglected.

The two-dimensional curvature effect. Field enhancement by surface roughness increases the effective fields. The surface roughness due to the atomic structure as displayed by scanning tunnelling microscopy is well known. For greater distances between cathode and anode the *atomic* roughness does not play a role. However, a possible unintended *microscopic* roughening of silicon interfaces can have enormous effects on the current. The effective barrier heights can be lowered considerably.

Trap-assisted tunnelling. Interface traps act like stepping stones for tunnelling

electrons. By modern processing techniques the number of interface traps can be reduced to a negligible amount. However, by the energy dissipation of electrons drifting from cathode to the anode, new interface states can be generated, which affect the barrier height. This will be discussed later.

(ii) *The Fowler–Nordheim equation for thick oxides*

To come to the classical Fowler–Nordheim equation we have to account for the energy distribution of electrons in the cathode. Thermal energy affects not only the average of the energy distribution, and hence the probability of passing the barrier, but also the width of the distribution, i.e. the number of electrons with higher energy than average. The pre-exponential, $J_{\max}$, may be regarded as the maximum current which would flow through the barrier if tunnelling were not a restriction. This term is also sensitive to the amount and energy levels of the charges at the interface. Hence it also depends on temperature, band bending, image charge effect, curvature of the interface and the number of interface traps. To keep things simple we will derive the Fowler–Nordheim equation in the first instance, neglecting the ballistic effects of electrons reflecting from the anode, band bending effects, surface roughness, image force and interface states.

The electrons able to pass the barrier all originate from energy levels close to the Fermi level. We therefore can expand the exponential term in a series expansion at $E = \Phi_b$, neglecting terms with $(E-\Phi_b)^2$ and higher powers. This alters equation (2.6) to

$$\mathrm{Prob}(E) = \exp\left[-\frac{4\sqrt{2m_{ox}\Phi_b^3}}{3\hbar\mathcal{E}q}\left(1+\frac{\Phi_b - E}{2\Phi_b}\right)\right]. \tag{2.8}$$

The transition probability peaks sharply at $E = \Phi_b$ and is very small for values $E \ll \Phi_b$.

The supply of electrons at an energy level between E and $E + \mathrm{d}E$ is given by the Fermi–Dirac distribution:

$$N(E)\,\mathrm{d}E = \frac{m_{cat}}{2\pi^2\hbar^3}kT\ln(1+\mathrm{e}^{-(E-\Phi_b)/kT})\,\mathrm{d}E \overset{kT\ll|\Phi_b-E|}{\longrightarrow} \frac{m_{cat}}{2\pi^2\hbar^3}(\Phi_b - E)\,\mathrm{d}E, \tag{2.9}$$

where the approximation in the last equation is allowed for $\Phi_b - E \gg kT$. Note that the temperature T drops out of the supply function, which makes the tunnel current, in the first instance, independent of temperature. It has been shown that the same Fowler–Nordheim equation is obtained when the total energy distribution is taken into account. The supply function $N(E,U)\,\mathrm{d}E\,\mathrm{d}U$ is equal to the number of electrons within the range U to $U + \mathrm{d}U$, the x-part of which lies in the range E–$E + \mathrm{d}E$. The probability for passing the barrier is the same (Van Oostrom 1965).

The Fowler–Nordheim equation. The tunnelling current is calculated by integrating the supply of electrons times the probability of passing the barrier:

$$\begin{aligned} J_{FN} &= q\int_0^\infty N(E)\,\mathrm{Prob}(E)\,\mathrm{d}E \\ &= q\frac{m_{cat}}{2\pi^2\hbar^3}\int_0^\infty(\Phi_b - E)\exp\left[-\frac{4\sqrt{2m_{ox}|\phi_b|^3}}{3\hbar\mathcal{E}q}\left(1+\frac{\Phi_b-E}{2\Phi_b}\right)\right]\mathrm{d}E \\ &= q^3\frac{m_{cat}\mathcal{E}^2}{16\pi^2\hbar m_{ox}|\Phi_b}\exp\left[-\frac{4\sqrt{2m_{ox}|\phi_b|^3}}{3\hbar\mathcal{E}q}\right]. \end{aligned}$$

PHILOSOPHICAL TRANSACTIONS OF THE ROYAL SOCIETY A MATHEMATICAL, PHYSICAL & ENGINEERING SCIENCES

This is the semiclassical Fowler–Nordheim equation. As stated, the WKB approximation neglects the secondary effects of very abrupt barriers. As shown by Jensen (1995) it overestimates the tunnelling probability for electrons at the band edge.

Band bending has to be taken into account. The temperature effect drops out by the assumption that $|\Phi_b - E| \ll kT$. In reality the supply function is not really temperature independent. The two-dimensional curvature effects must be taken into account. However, all these corrections are negligible compared to effects of the interface chemistry (Weinberg 1983).

For quantitative calculations of the Fowler–Nordheim current we refer to the recent comparison of miscellaneous calculations including the WKB approximation, modified WKB approximation, Wigner distribution functions and the exact solution in terms of Airy functions in an overview by Jensen & Ganguly (1993).

(c) *Field emission in ultrathin dielectrics*

Above 80 Å the transmission of an electron through the barrier is hardly affected by further events in the oxide conduction band. The electrons lose their energy on their way to the anode and a neglible fraction, when reflected, has sufficient energy to return to the tunnelling position.

Below 80 Å an increasing number of electrons, when reflected, can interfere with the incident wavefunction. To model this, exact solutions of the Schrödinger equation have to be used. However, the Schrödinger equation only accounts for the undamped propagation of the electrons in the barrier. Hence, the calculated results are not realistic in so far that they exaggerate the influence of quantum interference for thick dielectrics. In reality the electrons lose energy in the conduction band. Hence, for thick dielectrics $d > 80$ Å, the semi-classical Fowler–Nordheim equation (2.6) can better be used.

The exact solution for the transition coefficient in terms of Airy functions $\mathrm{Ai}[z]$ and $\mathrm{Bi}[z]$ and their derivatives $\mathrm{Ai}'[z]$ and $\mathrm{Bi}'[z]$ has been given by Gundlach (1966):

$$\begin{aligned} P_{\mathrm{Airy}} = \frac{k_{\mathrm{cat}}}{k_{\mathrm{an}}}\frac{4}{\pi^2}\{&[(k_{\mathrm{ox}}/k_{\mathrm{an}})(\mathrm{Ai}'[k_{\mathrm{ox}}]\,\mathrm{Bi}'[-k_{\mathrm{ox}}x_{\mathrm{l}}] - \mathrm{Ai}'[-k_{\mathrm{ox}}x_{\mathrm{l}}]\,\mathrm{Bi}'[k_{\mathrm{ox}}x_{\mathrm{t}}]) \\ &+(k_{\mathrm{cat}}/k_{\mathrm{ox}})(\mathrm{Ai}[k_{\mathrm{ox}}x_{\mathrm{t}}]\,\mathrm{Bi}[-k_{\mathrm{ox}}x_{\mathrm{l}}] - \mathrm{Ai}[-k_{\mathrm{ox}}x_{\mathrm{l}}]\,\mathrm{Bi}[k_{\mathrm{ox}}x_{\mathrm{t}}])]^2 \\ &+[(k_{\mathrm{cat}}/k_{\mathrm{an}})(\mathrm{Ai}[-k_{\mathrm{ox}}x_{\mathrm{l}}]\,\mathrm{Bi}'[k_{\mathrm{ox}}x_{\mathrm{t}}] - \mathrm{Ai}'[k_{\mathrm{ox}}x_{\mathrm{t}}]\,\mathrm{Bi}[-k_{\mathrm{ox}}x_{\mathrm{l}}]) \\ &+(\mathrm{Ai}[k_{\mathrm{ox}}x_{\mathrm{t}}]\,\mathrm{Bi}'[-k_{\mathrm{ox}}x_{\mathrm{l}}] - \mathrm{Ai}'[-k_{\mathrm{ox}}x_{\mathrm{l}}]\,\mathrm{Bi}[k_{\mathrm{ox}}x_{\mathrm{t}}])]^2\}^{-1}, \end{aligned} \tag{2.10}$$

where

$$k_{\mathrm{an}} = \sqrt{2m_{\mathrm{an}}E_{\mathrm{F}}/\hbar^2}, \quad k_{\mathrm{cat}} = \sqrt{(2m_{\mathrm{cat}}(\Phi_b + q\mathcal{E}x_{\mathrm{l}})/\hbar^2}, \quad k_{\mathrm{ox}} = \sqrt[3]{2m_{\mathrm{ox}}q\mathcal{E}/\hbar^2},$$

$x_{\mathrm{t}} = \Phi_b/q\mathcal{E}$ is the tunnel distance and $x_{\mathrm{l}} = d - x_{\mathrm{t}}$ is the effective length of the trajectory in the conduction band. E_{F} is the Fermi energy, m_{ox} is the electron mass in the oxide, m_{an} the effective electron mass in the anode and m_{cat} the effective electron mass in the cathode. Plotting $\Delta\Phi_b = \frac{2}{3}\log(P_{\mathrm{Airy}}/\mathrm{Prob})$, i.e. the variation of the barrier height with $\mathcal{E}$, displays the quantum oscillations. The theoretical oscillations are shown by the full line in figure 4.

(d) *Quantum oscillations in ultrathin dielectrics*

Silicon dioxide layers 30 Å$< d <$80 Å show an additional modulation of the current (Lewicki & Maserjian 1975; Fisschetti & DiMaria 1988; Zafar *et al.* 1995) caused by quantum-interference effects which are described by equation (2.10).

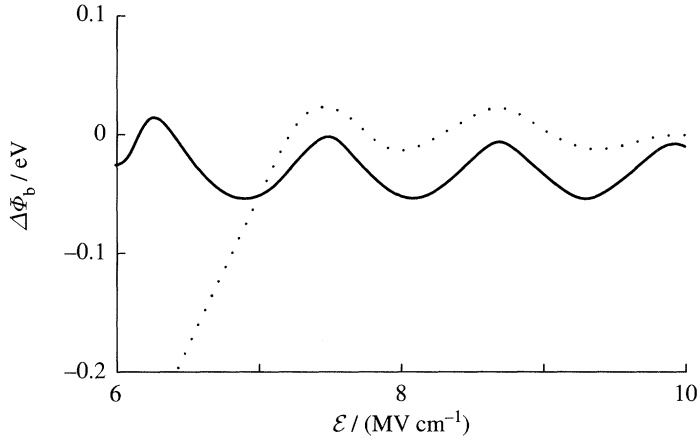

Figure 4. The amplitude of quantum oscillations is clearly visible when plotted as the experimental barrier height calculated by equation (2.4) versus the applied field. The modulation of the barrier height calculated with equation (2.10) but multiplied by a factor 0.1 has been added for comparison. 5.8 nm oxide; ·····, measurement; ——, equation (2.10).

The amplitude of the oscillation increases with decreasing oxide thickness. Below 30 Å, however, the direct tunnelling component overwhelms the Fowler–Nordheim current and the current becomes independent of field.

Quantum oscillations are clearly exhibited when presented as variations of the effective barrier height with field and are shown in figure 4. Note that, except for the amplitude, the Airy-curve fits well to the measured data. For this we had to add 6 Å to the thickness as determined by capacitative measurements. The phase and frequency of the oscillations are very sensitive to small variations of d. A small increase or decrease of d directly gives a large shift in phase and changes the frequency. Therefore, these oscillations are very well suited to determine the oxide thickness of ultra thin oxides. The correction of 6 Å is consistent with calculations of the charge density close to the interface (Jensen 1993). The charge density rapidly vanishes between 6 Å and the interface.

The mechanism of quantum oscillations has been revealed and fully described by Maserjian and co-workers (Maserjian 1988), assuming ballistic transport in the conduction band. The thicker the dielectric the more the waves damp out and the less is left of the interference effect. From the thickness dependence of the amplitude of the oscillations Lewicki & Maserjian (1975) and Zafar *et al.* (1995) estimated the energy relaxation length to be $\lambda = 6$ Å. Since this is, to our knowledge, the most direct way of observing the energy relaxation length, these results are extremely important. The results of Lewicki and Zafar are shown in figure 5. We have added our own results but find smaller amplitudes of the oscillations, and a relaxation length which is close to 11 Å. The reason for this is not quite clear, but may be due to enhanced surface roughness.

The implication of the short relaxation length is that only a vanishingly small fraction of injected electrons are expected to reach high energies in thick dielectrics. Even at fields up to 12 MV cm^{-1} average energies of electrons in the oxide conduction band will be below $\bar{E} = \lambda\mathcal{E} < 1$ eV. Although the energy loss of electrons in the conduction band is high and the quantum energy of emitted Bremsstrahlung is small, the situation changes when electrons drop to the Fermi level of the anode. Here they

PHILOSOPHICAL TRANSACTIONS OF THE ROYAL SOCIETY A MATHEMATICAL, PHYSICAL & ENGINEERING SCIENCES

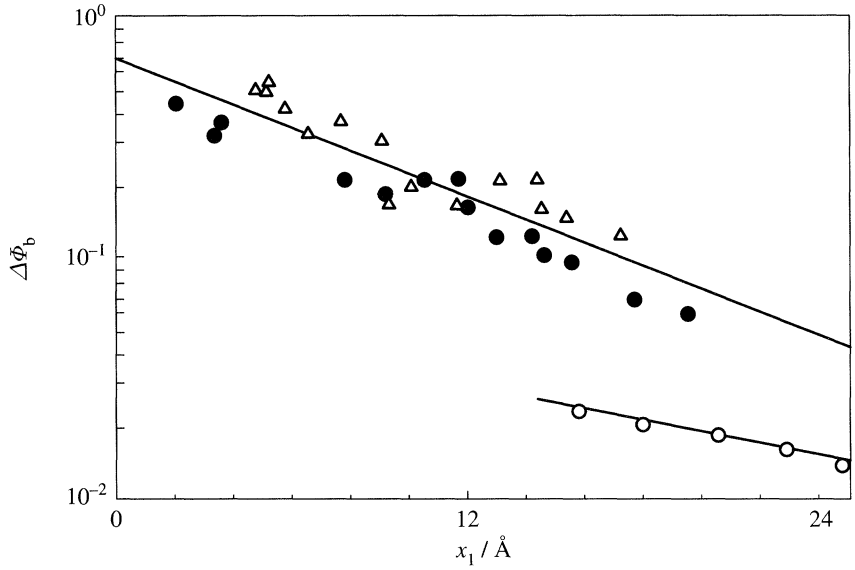

Figure 5. The amplitude of quantum oscillations decreases semilogarithmically with x_1, which is the oxide thickness minus the tunnel distance. After data from Lewicki & Maserjian (1975) and Zafar *et al.* (1995). Our own data show much smaller oscillations with an interaction length of about 13Å. △, Data from Lewicki; •, data from Zafar; ○, our data.

lose at least 3 eV. This energy drop can cause plasmons in the anode charge. A lot of work on the modelling of electron trajectories has been done by the IBM group (Fisschetti & DiMaria 1988).

3. Side effects of field emission

The main side-effects of field emission in dielectrics are:
(i) substrate currents which can be measured by carrier separation techniques;
(ii) light emission;
(iii) irreversible change of properties; and
(iv) irreversible breakdown.
Since the first two are closely related to the field emission itself, these will be discussed first. The last two will be discussed separately.

(*a*) *Substrate currents caused by field emission*

Eitan & Kolodny (1983), separating electron and hole currents in p-type substrates by appropriate p–n structures, observed a substrate current due to holes. The hole currents are closely related to the electron tunnelling current. The hole current is a fraction of the tunnel current and tracks the Fowler–Nordheim curve but with a barrier height of 3.8–4 eV. It was therefore attributed to electrons tunnelling from the valence band into the conduction band of the oxide and leaving a hole in the valence band. This is depicted in figure 6.

Weinberg & Fischetti (1985) investigated this phenomenon in detail and found Eitan's model inconsistent with J_{max} values as expected for tunnelling through a 4 eV barrier. In fact, the observed value is orders of magnitude too high. A number of alternative explanations have been proposed in the literature based on hole tunnelling (Satake & Toriumi 1995) and valence-band tunnelling (Chao & Chen 1995). As an

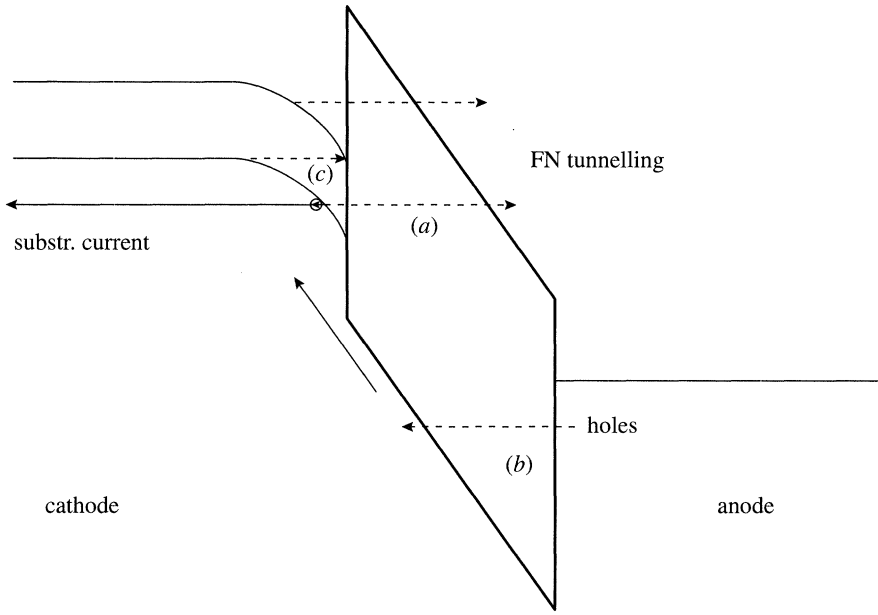

Figure 6. The existing models for substrate currents: (*a*) an electron tunnelling from the cathode valence band; (*b*) a hole tunnelling from the anode in the oxide valence band; (*c*) band-to-band tunnelling.

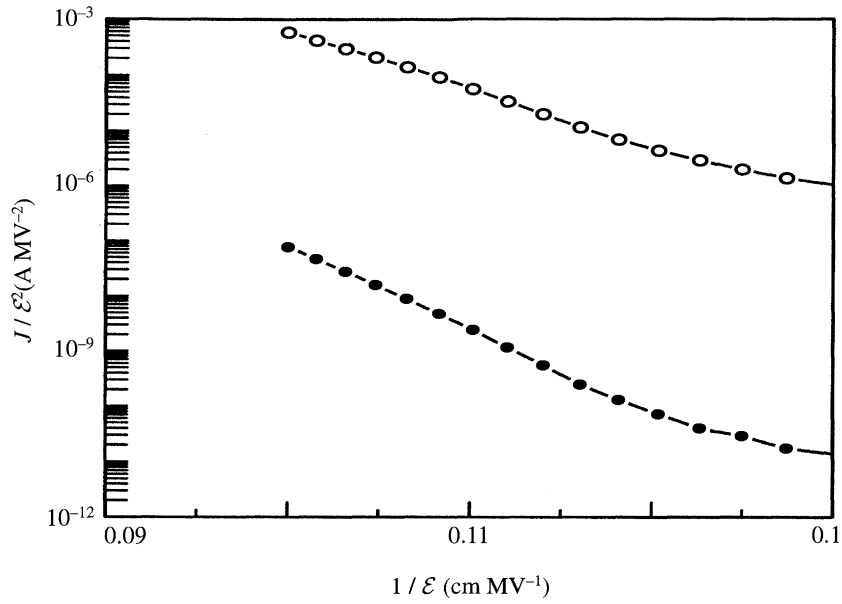

Figure 7. Fowler–Nordheim plot of the tunnel and substrate currents. 5.8 nm; ○, Fowler–Nordheim; ●, substrate current.

example we show the Fowler–Nordheim plots of the tunnel and substrate currents in figure 7.

It appeared interesting to check whether the quantum oscillations can also be detected in the substrate current. The extraction technique plotting the barrier height,

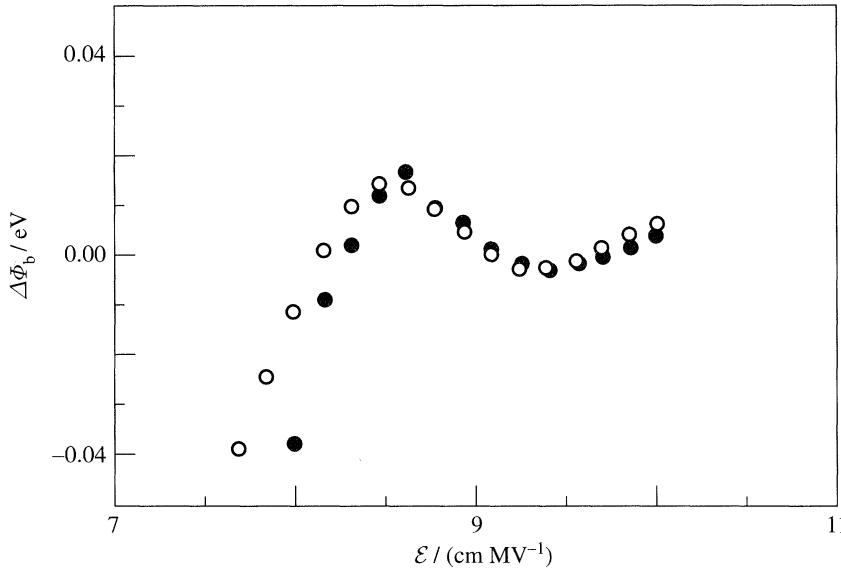

Figure 8. Quantum oscillations in Fowler–Nordheim currents and substrate currents. Note that the oscillations are coherent with those in the Fowler–Nordheim currents. This aspect is very important for the interpretation of the substrate currents. 5.8 nm; ○, Fowler–Nordheim; ●, substrate current.

$\beta(\mathcal{E})$, against field reveals that for thin oxides substrate currents are indeed modulated by 'quantum oscillations'. This is shown in figure 8. Although the currents are low and modulations on the low currents are not easy to detect, the quantum oscillations are very well established. We observed quantum oscillations for several oxide thicknesses in the range from 40–60 Å.

The remarkable aspect of these modulations is that they are completely 'coherent' with the Fowler–Nordheim currents. This unexpected behaviour rules out explanations based on anode hole tunnelling and electron tunnelling from the valence band. Electrons tunnelling from the valence band should have a difference in 'phase'. Holes in the oxide valence band have a different mass and different starting point, hence 'frequency' and 'phase' would be different. Band-to-band tunnelling, when considered as an independent process, would have no oscillations at all.

(*b*) *Light caused by field emission*

Fowler–Nordheim currents in dielectrics emit light. This light is clearly visible when remote electrodes are used. In gated MOS capacitors, however, the light is mainly absorbed in the polysilicon gate, but with sensitive photomultipliers it can be detected and even its distribution over the area can be measured.

As an example, the light emitted by a Fowler–Nordheim current passing through a 60 Å oxide is shown in figure 9. When corrected for the auto-absorption the intensity of the light is observed to decrease with frequency above 3 eV.

The intensity of the light emission of electrons in dielectrics can be written as a function of fluctuations of the Fowler–Nordheim current. The intensity of the light and its spectral distribution is then given by the autocorrelation of the Fowler–

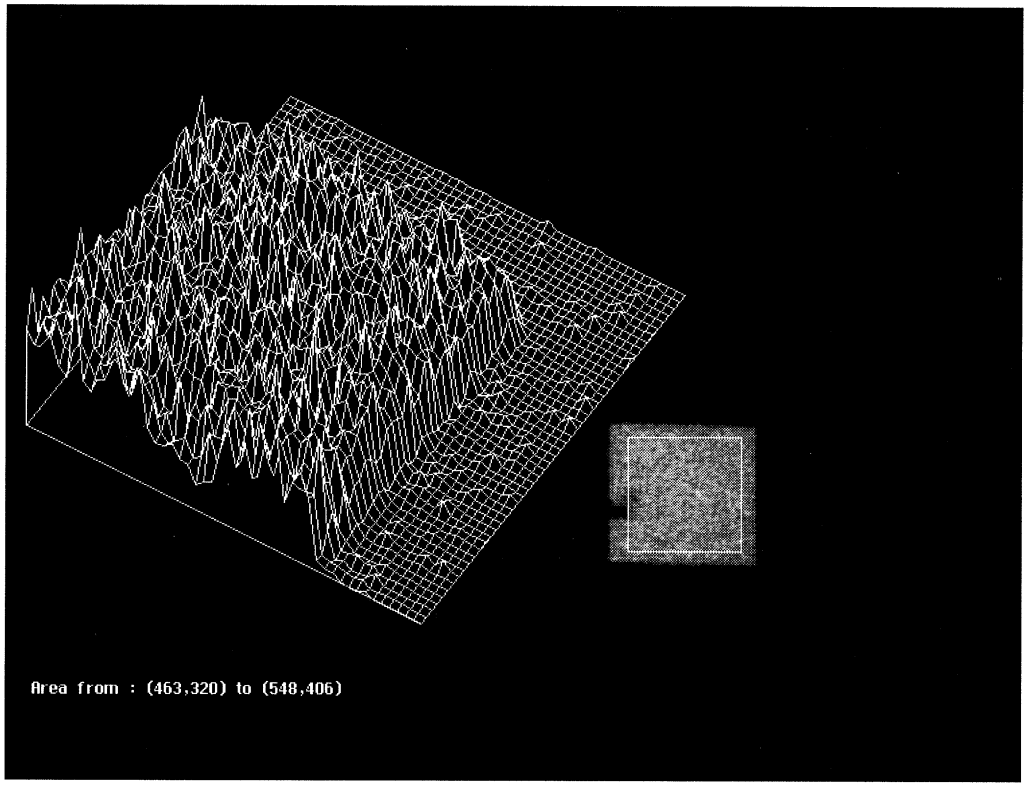

Figure 9. Spatial distribution of photon emission by Fowler–Nordheim currents.

Nordheim current, as shown by Uehara and co-workers (Uehara *et al.* 1995):

$$|I(\omega)|^2 \propto qJ_{\mathrm{FN}} \left\{1 + \sqrt{\frac{\hbar\omega}{q\Phi_{\mathrm{b}}} + 1}\right\}^{-2} \exp\left[\frac{-\beta}{2\mathcal{E}}\left\{\left(\frac{\hbar\omega^{3/2}}{q\Phi_{\mathrm{b}}}\right) - 1\right\}\right]. \qquad (3.1)$$

At $\omega = 0$ the light intensity is proportional to the product of tunnelling current and elementary charge q, i.e. the dissipated power. This equation holds for the situation where the scattering is mainly in the conduction band. When the anode interface is not completely smooth, a surface–roughness-mediated light intensity can affect the validity of equation (3.1). Quantitative correlations between light emission and electric power consumption in light emitting *pn*-junctions were published by deKort *et al.* (1993).

4. The irreversible effects of field emission

Charge injection leads to severe degradation of the dielectric and even small amounts of charge may affect the properties of the MOS capacitor. First, we shall discuss the effects on the intrinsic properties of the dielectric. These are the lowering of the effective tunnelling barrier and the increase of dielectric losses. Then severe degradation will be examined.

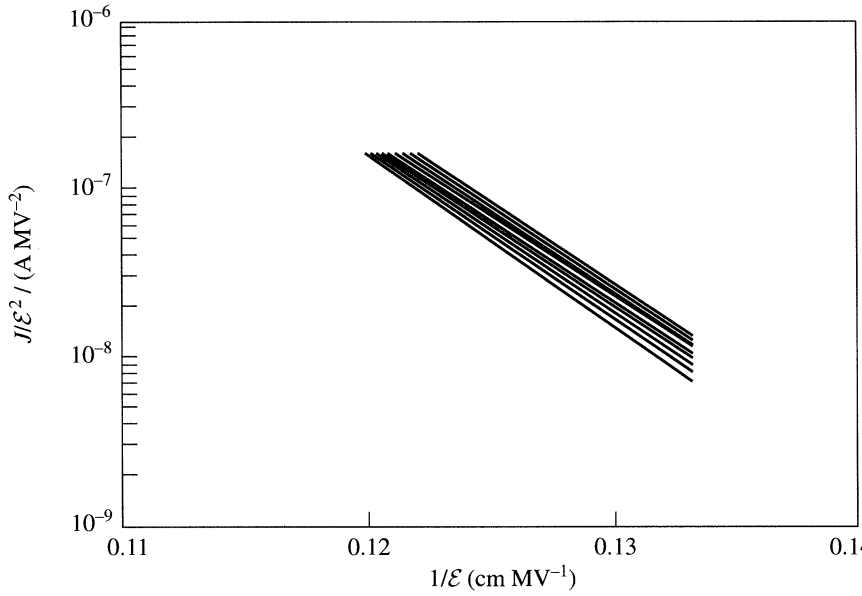

Figure 10. Series of Fowler–Nordheim plots of virginal and stressed capacitors. 28 nm oxide.

(*a*) *Reduction of the Fowler–Nordheim barrier*

In the following it will be shown that even after low fluences, such as $Q_{\mathrm{inj}} = 10^{-6}$ C cm^{-2}, a dielectric can show degradation. Many papers have investigated changes in the space-charge density due to stressing, and many have dealt with a systematic treatment of the Fowler–Nordheim curve. Not many have investigated the effect whereby the injection of charges degrades the barrier height (Wolters & Zegers-van Duijnhoven 1987*b*). Figures 10 and 11 shows how the Fowler–Nordheim curves shift for a very small fluence of electrons. The effective barrier height is plotted against the fluence of electrons for two stressing conditions. As can be seen, the degradation starts at a fluence as low as 10^{-6} C cm^{-2}. Obviously, the lowering of the barrier height is substantially larger when a stress current of 10^{-2} A cm^{-2} is used instead of 10^{-3} A cm^{-2}. The critical charge needed for a shift is, however, practically the same. These shifts towards lower barrier height are often mistaken for an evolution of positive charge in the dielectric. The mechanism responsible for the lowering of the barrier is the generation of interface traps. These give rise to trap-assisted tunnelling (Wolters & Zegers-van Duijnhoven 1987*b*).

(*b*) *The increase of dielectric losses*

Many papers (Lai & Young 1981; Nissan-Cohen *et al.* 1985*a*, *b*; Harrari 1978; Dimaria & Fischetti 1987) have documented the generation of traps which can be measured by the distortion of *C*–*V* curves. One of the most sensitive techniques consists of measuring the dielectric loss of a MOS capacitor. An example of losses generated by injected charge is given in figure 12.

As can be seen, losses continuously increase by charge injection. In most cases these losses are interpreted as being caused by interface states. The atomic picture of what is happening, however, is not clear (Fisschetti *et al.* 1985). This is why we will focus on the mesoscopic effects of charge injection.

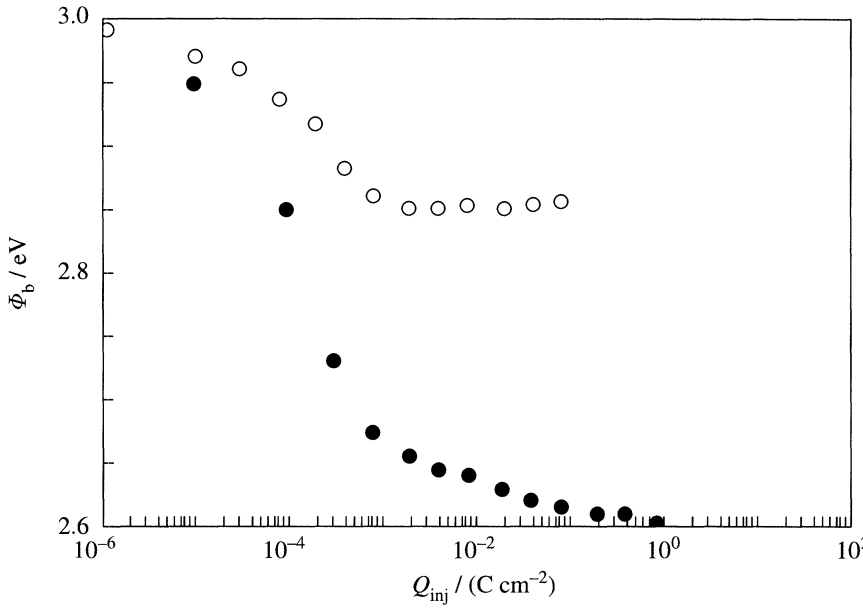

Figure 11. The Fowler–Nordheim barrier height degrades as a function of charge injection. ○, J_{stress} 10^{-3} A cm^{-2}; ●, J_{stress} 10^{-2} A cm^{-2}.

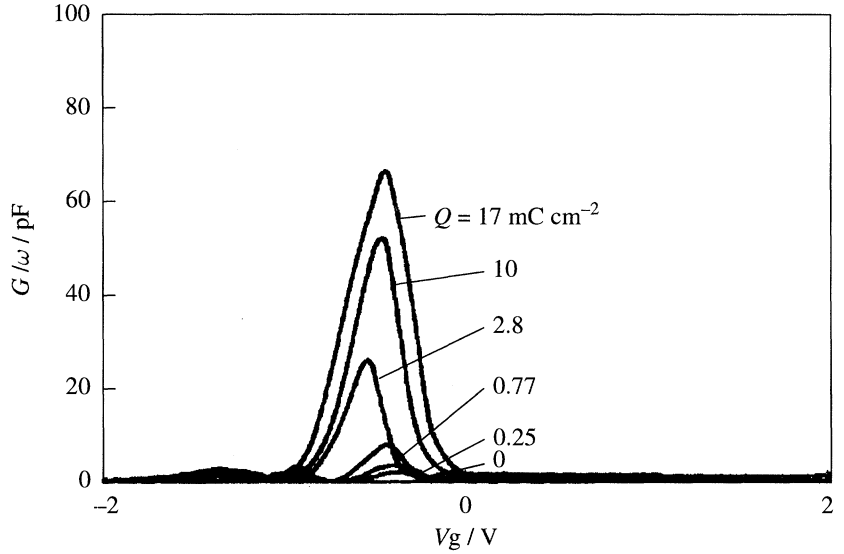

Figure 12. The increase of the dielectric loss, G/ω, where G is the conductance, as a function of gate voltage with charge transport through the dielectric as a parameter. Poly-Si stress (+); oxide 281 Å; n-type Si; frequency is 100 kHz.

(*c*) *Severe degradation of the dielectric*

Properties of a dielectric change when a charge flux is sustained for some time. *C–V* and *I–V* analysis show that these changes comprise:

(1) change of the barrier height (interface traps);
(2) negative space charge (trapping);
(3) positive space charge (hole trapping or trap generation);

(4) increased AC-losses (interface state generation?);
(5) polarization effects (generation of slow states?); and
(6) dielectric breakdown.

The degradation by charge injection eventually causes breakdown. This occurs when sufficient charge has been injected (Wolters 1981*a*). The degradation of the dielectric is related to the growth of *mesoscopic features* which form low-ohmic paths between anode and cathode. The generation of such paths is obviously related to the energy dissipation of electrons. The energy dissipation may cause plasmons in the anode and photons, but may also cause irreversible changes within a distance of the energy-absorption length, λ_{abs}.

The damage generated by the energy explosion of an electron can therefore be at a distinct distance, λ_{abs}, from the location where it is injected in the anode. For $h\omega = 3\,\mathrm{eV}$ this distance can be $\lambda_{\mathrm{abs}} \sim 2500\,\text{Å}$, which comes in the order of the dimensions of our smallest devices. In any case it is a multiple of the thickness of the gate oxide. This means that damage can be generated relatively far from the place the electron loses its energy.

(*d*) *Mesoscopic features in the dielectric*

By mesoscopic features we mean damage which is spread out over several atomic distances. In thick dielectrics these features have the shape of 'trees'. These 'trees' grow from anode to cathode and lead eventually to a breakdown path. The first path starting at the anode and contacting the cathode releases the stored energy in the capacitor.

The generation of a mesoscopic feature and eventually a low resistance path is depicted in the following steps (1)–(6), which correspond to parts 1–6 in figure 13.

(1) When electrons generate broken bonds at the cathode the network can rupture over a region 1–2 nm into the dielectric. A state in this ruptured region may be observed by barrier lowering.

(2) When traps are formed deeper than 5 nm from the cathode they may be filled permanently and form a negative space charge which locally inhibits further injection.

(3) When a bond is broken at the anode, the interface trap can be positively charged. This charge attracts newly injected electrons which dissipate their conduction band energy close to the same location. This confines the energy dissipation to the damaged region. The region will protrude further into the dielectric and attract still more electrons, etc. If the region extends to locations more than 3 nm from the anode, a fixed positive charge may be formed. Charge can easily be exchanged with the electrode since the dielectric in between contains traps as well.

(4) Charge transport via channels to places deeper in the dielectric gives rise to losses at high frequencies (cf. figure 12). If the channels increase in length the resonance frequency will decrease. Slow states are formed. The longer channels attract electrons more efficiently because of their positively charged tips and this confines further energy dissipation and localizes the degradation of the dielectric.

(5) When the channels, containing a large number of states, protrude into the dielectric their charge content can increase in a strong field. The field is especially large when the channel is close to the counter-electrode. The saturation level of the traps thus becomes field-dependent and the space charge in the dielectric, which can no longer be so easily exchanged, causes hysteresis effects.

(6) Finally, the channels reach the cathode within the tunnelling distance and the

PHILOSOPHICAL TRANSACTIONS OF THE ROYAL SOCIETY A MATHEMATICAL, PHYSICAL & ENGINEERING SCIENCES

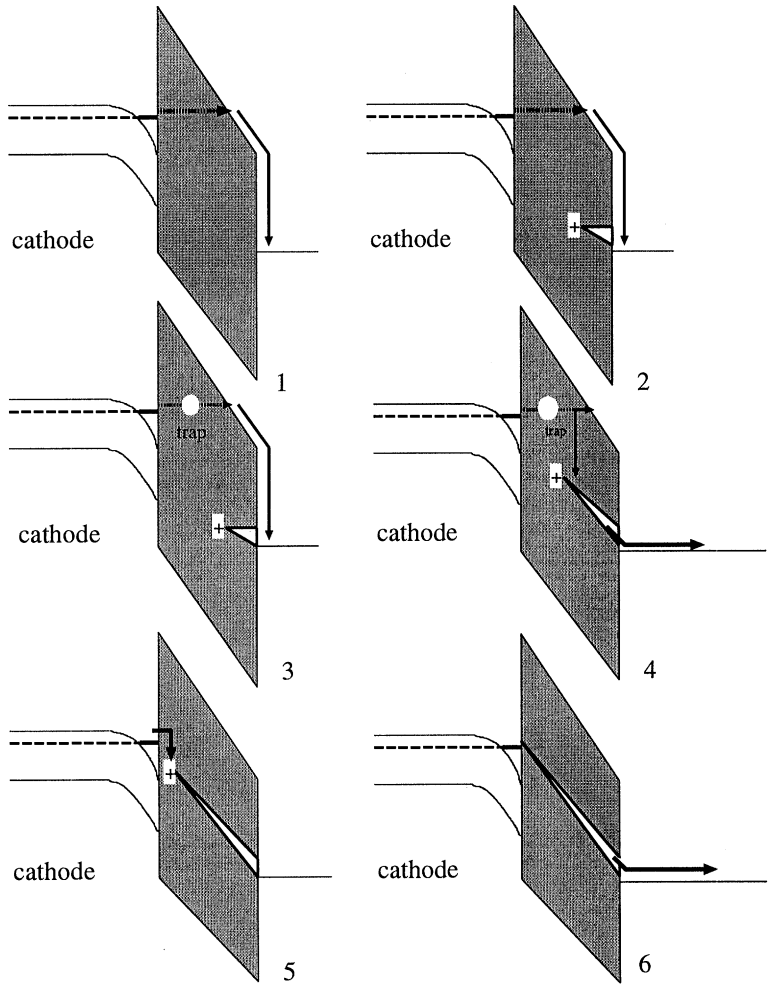

Figure 13. (1) Fowler–Nordheim injection of electrons. (2) The generation of broken bonds at the interface. (3) Electrons can penetrate the barrier by trap-assisted tunnelling. Traps located more than 5 nm from the electrodes can be filled permanently. (4) Traps at the anode interface will be charged positively and attract electrons. The confinement of energy dissipation can cause traps to be formed deeper into the dielectric. This generates a channel. (5) The channels grow and reach the region close to the cathode. (6) Once the path reaches the cathode, the capacitor can discharge its energy $\frac{1}{2}CV^2$.

total energy of the biased capacitor, $\frac{1}{2}CV^2$, can be discharged. This fast adiabatic process can burn a hole in the capacitor.

(*e*) *Computer modelling of 'trees'*

We have modelled the growth of the 'trees' by computer. Electrons are randomly injected one by one from the cathode. Step by step their trajectories are calculated by Coulomb's law. The first electron moves directly to the anode. At the anode it is assumed that it can produce a trap which is positively charged. The next electron's trajectory is affected by this extra positive charge. After a number of injections an electron may enter an earlier generated trap. This extends the trap in the direction from which the electron came. By continuous random injection the number of traps

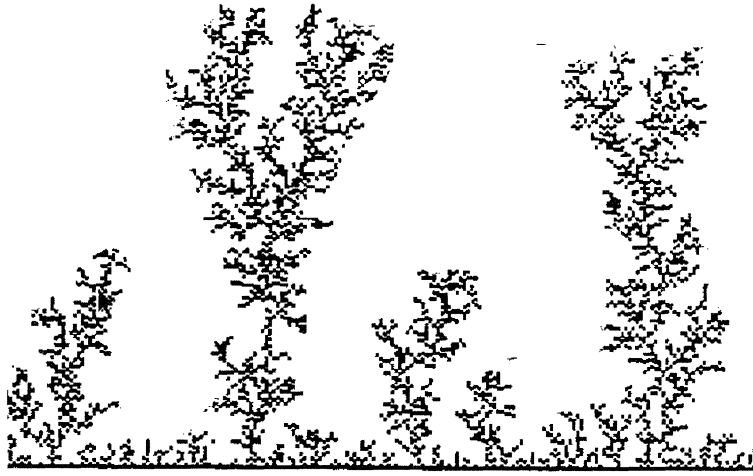

Figure 14. The computer modelling of mesoscopic features or 'trees' leading to degradation and breakdown.

grow (mesoscopic features) in the direction of the cathode, bifurcating when charge comes from different directions. The mesoscopic features grow like 'trees', as shown in figure 14. After sufficient injection a breakdown is produced. The results look like 'trees' which can be made visible in thick dielectrics (Wolters & van der Schoot 1985*d*).

5. Breakdown by degredation

It will be clear that a large number of injected charges are needed to generate the mesoscopic features leading to breakdown. This has led to the formulation of the Q_{bd} model for breakdown (Wolters 1981*d*). The model assumes that breakdown is the end of a degradation process. Since all electrons dissipate at the anode (Wolters & van der Schoot 1985*a*, *b*, *c*, *d*, 1986), with at least 3 eV the degradation is mainly determined by the number of charges injected in the anode rather than the dissipation in the conduction band. The field is, however, needed to inject the charges. For thicker samples we have shown that it makes no difference whether we use a constant-current or -voltage or ramping-current or -voltage method to measure breakdown. This can be seen in figure 15, where we have plotted the fraction of broken down capacitors $F = n/(N+1)$, where n is the number of failed capacitors and N the total number of tested capacitors versus $\log Q_{\mathrm{bd}}$ on probability paper (Wolters 1985*b*).

All stress methods lead to similar distributions on a probability plot. The tails at low values of F are caused by defects. The important condition for coinciding distributions is that currents and fields at breakdown are not very different.

The Q_{bd} model appears to hold for oxide layers down to 40–60 Å, as we can see in figure 16. For a large range of current densities the Q_{bd} values decrease slowly with injection current.

(*a*) *Energy dissipation in the prebreakdown stage*

The energy stored and dissipated in the capacitor before breakdown can best be illustrated by a plot of the total charge density, Q, needed to apply a voltage, V, across the capacitor. This is depicted in figures 17*a* and *b*. These figures can be compared with a stress–strain plot as used for mechanical breakdown (Wolters &

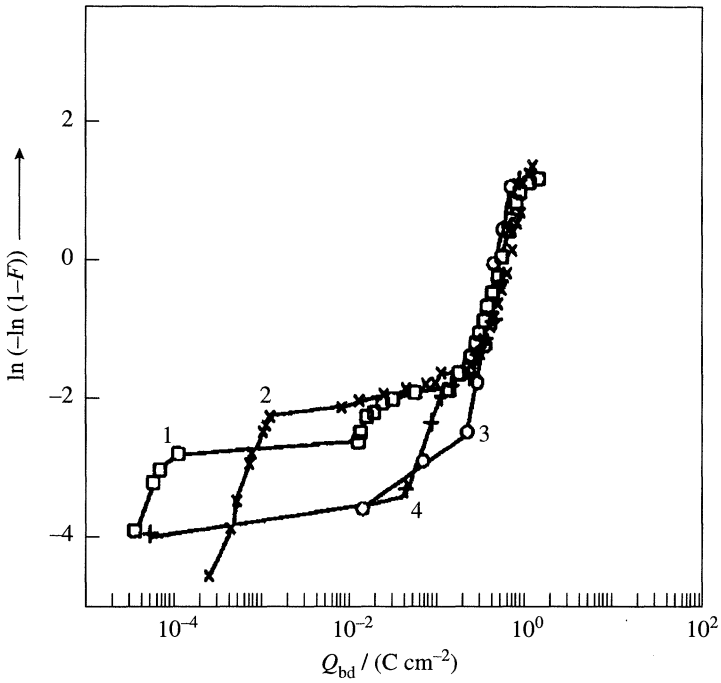

Figure 15. Different stress methods lead to similar Q_{bd} distributions for breakdown. F is the cumulative probability of failure for a set of capacitors. At low values of F, distributions show tails caused by defects. 1, Constant current; 2, constant voltage; 3, ramped voltage; 4, ramped current; poly-Si; 110 Å oxide; p-substrate Si.

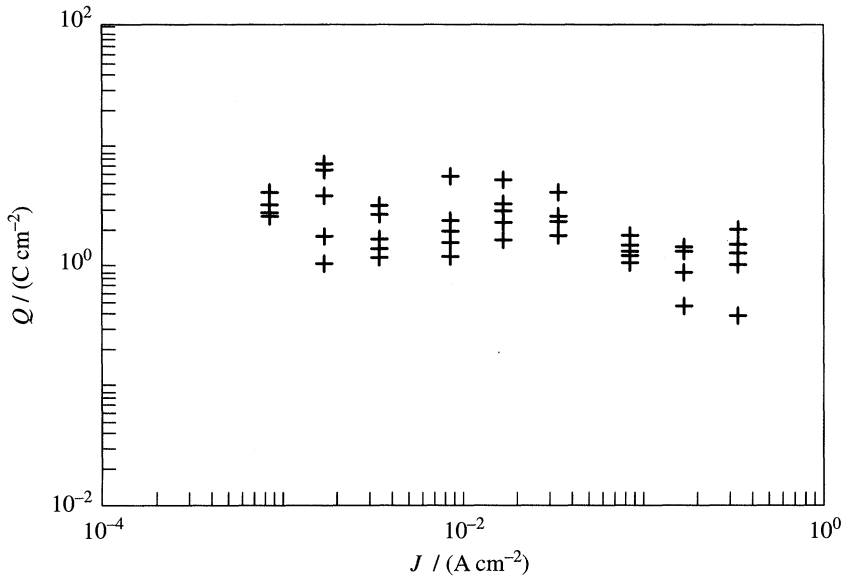

Figure 16. Average Q_{bd} values as a function of injection current. 5.8 nm oxide.

Van der Schoot 1985*b*). At low voltages, Q is practically equal to the displacement charge density, stored at the electrodes of the capacitor. The stored energy is equal to $\frac{1}{2}Q^2d/\epsilon_{ox}$.

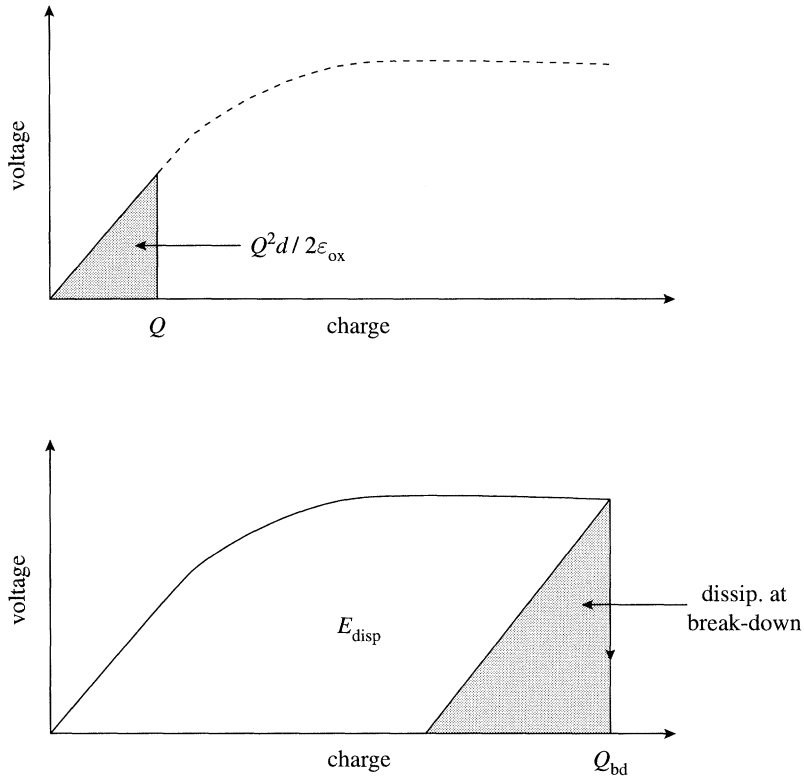

Figure 17. Stress–charge plot depicting the energy dissipation during stress and breakdown: (*a*) in the low voltage regime almost all energy can be recovered; (*b*) after substantial charge injection a lot of energy has been dissipated degrading the dielectric. The conservatively stored energy $\frac{1}{2}\epsilon_{ox}d\mathcal{E}_{bd}^2$ will be dissipated when breakdown occurs.

In the nonlinear part energy is dissipated by charge leakage through the dielectric. Under stress this energy increases continuously. The degradation generates 'trees' which grow between the electrodes. The growth continues until the two electrodes are connected and breakdown occurs (Wolters & Van der Schoot 1985*d*). At that point the displacement energy, still present in the capacitor, is dissipated.

(*b*) *Energy dissipation at the moment of breakdown*

When a low-resistance path is formed, by degradation of the dielectric, this path will eventually interconnect the two electrodes. The displacement charge on both electrodes recombines and then energy still stored in the capacitor (the shadowed area in figure 17*b*) is released in a very fast energy explosion. The displacement energy per area is given by

$$E_{disp} = \tfrac{1}{2}CV^2/A = \tfrac{1}{2}\mathcal{E}_{bd}^2 d\epsilon_{ox}, \tag{5.1}$$

where A is the area of the capacitor, $\mathcal{E}_{bd}$ the applied field at breakdown and ϵ_{ox} the dielectric constant of the oxide film. It is this energy, E_{disp}, which causes the visible damage after breakdown. The energy dissipation is so fast that the capacitor partly melts and evaporates, and a sort of crater is formed by which the capacitor can be shorted.

For a field of 10 MV cm^{-1} and $d = 300$ Å and a capacitor with an area of 1 mm^2,

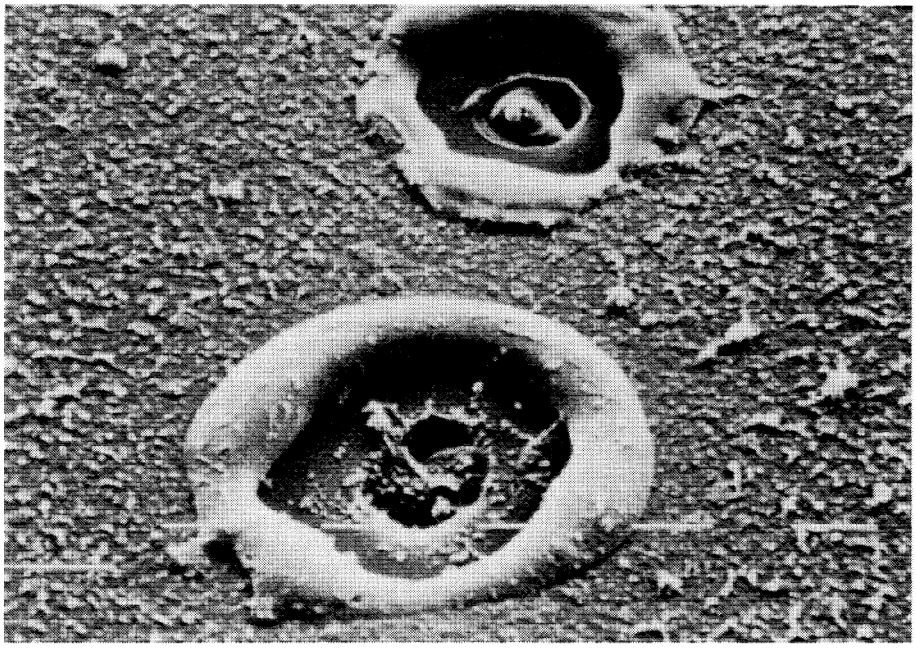

Figure 18. The final breakdown of a capacitor leaves a crater, whose dimensions can be calculated from the energy, $\frac{1}{2}CV^2$, stored in the capacitor just before breakdown. There are two craters because the first breakdown was self-healing, i.e. the shorting path has been removed by the breakdown. White bars correspond to a length of 1 μm.

the displacement energy is equal to 5.1×10^{-7} J. When this is dissipated in a point source, a sphere with a radius of 1 μm can be evaporated. The heat required to warm up and evaporate silicon is 4.2×10^5 J cm^{-3}. This value of 1 μm is about the diameter of the craters which are observed after a breakdown in MOS capacitors (Wolters & Van der Schoot 1985*a*). Figure 18 shows such craters formed in a capacitor of 1 mm^2. At low currents only one crater is formed. The breakdown can burn away the short, however, and after continued stress a second hole of almost equal dimensions is formed.

6. Conclusions

This paper overviews the phenomenon of field emission in silicon dioxide and the main side-effects including degradation and breakdown. In short the main points are as follows.

(i) The Fowler–Nordheim tunnel current has been discussed, in terms of tunnelling probability and supply currents.

(ii) The tunnelling probability can be increased by band bending, image force, two-dimensional curvature and traps.

(iii) In thin oxides the reflection of electrons against the anode can explain the oscillations superposed on the Fowler–Nordheim plots. The oscillations decrease with oxide thickness. Above 80 Å they can hardly be detected. The 'frequency' of quantum oscillations provides a good tool to determine the oxide thickness.

(iv) The side-effects of field emission, substrate currents and light emission have been discussed. Quantum oscillations in the substrate currents rebut existing models

based on anode hole injection and cathode-valence-band electron injection or band-to-band tunnelling.

(v) Irreversible effects of field emission are degradation and breakdown. The lowering of the barrier height, increase of losses and formation of mesoscopic features are aspects of the continuous degradation. Computer simulation shows 'trees' which grow from anode to cathode.

(vi) The energy dissipation needed for degradation and that for breakdown are discussed. It is shown that at breakdown the damage scales with the displacement energy which is stored in the capacitor.

We thank Henk Boots, Mare de Jong and Frans Widdershoven for intensive discussions, Ger Paulzen for samples and Harm Peters for light emission measurements. Leon Schmidt for programming the computer model.

The following list includes additional material not cited in the text.

References

Apte, P. P. & Saraswat, K. C. 1993 SiO_2 degradation with charge injection polarity. *IEEE Electron. Devel. Lett.* **14**, 512–514.

Chao, K. C. & Chen, M. J. 1995 Fowler–Nordheim limited band-to-band tunnelling for P-MOSFET gate current in a floating bulk condition. *Solid State Electron.* **38**, 135–137.

deKort, K., Damink, P. & Boots, H. 1993 Spectrum emitted by hot-electrons in p-i-n cold cathodes *Phys. Rev.* B **48**, 11912–11920.

DiMaria, D., Dong, D., Falcony, C., Theis, T., Kirtley, J., Tsang, X., Young, D., Pesavento, F. & Brorson, S. 1983 Charge transport and trapping phenomena in off-stoichiometric silicon dioxide films. *J. Appl. Phys.* **54**, 5801–5827.

Dumin, D. J., Mopuri, S. K., Vanchinathan, S., Scott, R. S., Subramoniam, R. & Lewis, T. G. 1995 High-field related thin oxide wearout and breakdown. In *IEEE Trans. Electron. Devel.* **42**, 760–772.

Dumin, D. J., Vanchinathan, S., Mopuri, S. K. & Subramoniam, R. 1995 Evidence for nonuniform trap distribution in thin oxides after high-voltage stressing. *J. Electr. Chem. Soc.* **142**, 2055–2059.

Elrharbi, S., Jourdain, M. & Meinertzhagen, A. 1994 Effect of the tunneling electrons in Fowler–Nordheim regime on the current voltage characteristics and model of degradation of metal-oxide-semiconductor capacitors. *J. Appl. Phys.* **76**, 1013–1020.

Eitan, B. & Kolodny, A. 1983 Two components of tunneling currents in metal-oxide-silicon structures. *Appl. Phys. Lett.* **43**, 106–108.

Faigon, A., Straboni, A., Miranda, E. & Redin, G. 1993 Tunneling in Al-silicon oxynitride structures. *Thin Solid Films* **230**, 133–137.

Fisschetti, M. V. & DiMaria, D. J. 1988 Hot electrons in SiO_2: ballistic and steady state transport. *Appl. Surf. Sci.* **31**, 375–389.

Fisschetti, M. V., Laux, S. E. & DiMaria, D. J. 1988 The physics of hot electron degradation of Si MOSFETs: can we understand it? *Appl. Surf. Sci.* **39**, 578–596.

Fowler, R. H. & Nordheim, L. 1928 Electron emission in intense fields. *Proc. R. Soc. Lond.* A **119**, 173–181.

Gundlach, K. H. 1966 Zur Berechnung des Tunnelstroms Durch eines Trapezeformige Potential Stufe. *Solid State Electron.* **9**, 949–957.

Harrari, E. 1978 Dielectric breakdown in electrically stressed thin films of thermal SiO_2. *J. Appl. Phys.* **49**, 2478–2488.

Hegarty, C. J., Lee, J. C. & Hu, C. M. 1991 Enhanced conductivity and breakdown of oxides grown on heavily implanted substrates. *Solid State Electron.* **34**, 1207–1213.

Hemink, G., Endoh, T. & Shirota, R. 1994 Modeling of the hole current caused by Fowler–Nordheim tunneling through thin oxides. *Jap. J. Appl. Phys.* **33**, 546–549.

PHILOSOPHICAL TRANSACTIONS OF THE ROYAL SOCIETY A MATHEMATICAL, PHYSICAL & ENGINEERING SCIENCES

Jensen, K. L. 1995 Improved Fowler–Nordheim equation for field-emission from semiconductors *J. Vac. Sci. Technol.* B **13**, 516–521.

Jensen, K. L. & Ganguly, A. K. 1993 Numerical-simulation of field-emission and tunneling – a comparison of the Wigner function and transmission coefficient approaches. *J. Appl. Phys.* **73**, 4409–4427.

Kobayashi, K., Teramoto, A., Hirayama, M. & Fujita, Y. 1995 Model for the substrate hole current based on thermoionic hole emission from the anode during Fowler–Nordheim electron-tunneling in the N-channel metal-oxide-semiconductor field effect transistors. *J. Appl. Phys.* **77**, 3277–3282.

Kong, S. O. & Kwok, C. Y. 1993 Fowler–Nordheim tunneling current in a Mg/polycrystalline Si oxide/N+ polycrystalline Si metal-oxide-silicon structure. *Appl. Phys. Lett.* **63**, 2667–2669.

Ku, P. S. & Schroder, D. K. 1994 Charges trapped throughout the oxide and their impact on the Fowler–Nordheim current in MOS devices. *IEEE Trans. Elec. Devel.* **41**, 1699–1672.

Lenzlinger, M. & Snow, E. H. 1969 Fowler–Nordheim tunneling into thermally grown SiO_2. *J. Appl. Phys.* **40**, 278–282.

Lewicki, G. & Maserjian, J. 1975 Oscillations in MOS tunneling. *J. Appl. Phys.* **46**, 3032–3039.

Mistry, K. & Doyle, B. 1995 How do hot carriers degrade N-channel MOSFETs. In *IEEE Circ. Devel. Magazine* **11**, 28–33.

Oostrom, A. G. J. van 1965 Validity of the Fowler–Nordheim model for field electron emission. Thesis, Amsterdam.

Pan, Y. 1994 A physical-based analytical model for the hot-carrier-induced saturation current degradation of P-MOSFETs *IEEE Trans. Elec. Devel.* **41**, 84–89.

Paskaleva, A. & Atanassova, E. 1993 Fowler–Nordheim tunneling injection in the Si–SiO_2 system treated with argon plasma. *Semicond. Sci. Technol.* **8**, 1566–1570.

Poler, J. C. 1994 Characterization of the Si/SiO_2 interface morphology from quantum oscillations in Fowler–Nordheim tunneling currents. *J. Vac. Sci. Technol.* B **12** 88–95.

Roh, Y., Trombetta, L. & Han, J. 1995 Analysis of charge components induced by Fowler–Nordheim tunnel injection in silicon-oxides prepared by rapid thermal oxidation. *J. Electr. Chem. Soc.* **142**, 1015–1020.

Satake, H. & Toriumi, A. 1995. Temperature-dependent hole fluence to breakdown in thin gate oxides under Fowler–Nordheim electron-tunneling injection. *Appl. Phys. Lett.* **66**, 3516–3517.

Schuegraf, K. F. & Hu, C. 1994 Metal-oxide-semiconnductor field-effect-transistor substrate current during Fowler–Nordheim tunneling stress and silicon dioxide reliability. *J. Appl. Phys.* **76**, 3695–3700.

Simoen, E. & Claeys, C. 1995 Substrate current characteristics in partially depleted silicon-on-insulator N-MOSFETs from room temperature down to 4.2 K. *Cryogenics* **35**, 321–326.

Uehara, Y., Watanabe, J., Fujikawa, S. & Ushioda, S. 1995 Light-emission mechanism of Si-MOS tunnel-junctions. *Phys. Rev.* B **51**, 2229–2238.

Uraoka, Y., Tsutsu, N., Morii, T., Nakata, Y. & Esaki, H. 1993 Hot carrier evaluation of MOSFETs in ULSI circuits using the photon emission method. *IEEE Trans. Elec. Devel.* **40**, 1426–1431.

Weinberg, Z. A. 1977 Tunneling of electrons from Si into thermally grown SiO_2. *Solid State Electron.* **20**, 11–18.

Weinberg, Z. A. 1982 On tunneling in metal-oxide-silicon structures. *J. Appl. Phys.* **53**, 5052–5056.

Weinberg, Z. A. 1983 Effect of silicon orientation and hydrogen anneal on tunneling from Si into SiO_2. *J. Appl. Phys.* **54**, 2517–2521.

Weinberg, Z. A. & Fisschetti, M. V. 1985 Investigation of the SiO_2-induced substrate current in silicon field effect transistors. *J. Appl. Phys.* **57**,443–452.

Weinberg, Z., Fischetti, M. & Nissan-Cohen, Y. 1986 SiO_2–induced substrate current and its relation to positive charge in field-effect transistors. *J. Appl. Phys.* **59**, 824–832.

Wolters, D. R. 1981*a* Breakdown and wearout in SiO_2. *Springer series in Electrophysics* (ed. M. Schulz & G. Pensl), vol. 7, pp. 180–194. Berlin: Springer.

PHILOSOPHICAL TRANSACTIONS OF THE ROYAL SOCIETY A MATHEMATICAL, PHYSICAL & ENGINEERING SCIENCES

Wolters D. R. & Verweij J. F. 1981*b* Charge trapping in SiO_2. *Springer Series in Electrophysics* (ed. M. Schulz & G. Pensl), vol. 7, pp. 111–117. Berlin: Springer.

Wolters, D. R. & van der Schoot, J. J. 1985*a* Kinetics of charge trapping in SiO_2. *J. Appl. Phys.* **58**, 831–837.

Wolters, D. R. & van der Schoot, J. J. 1985*b* Dielectric breakdown in MOS devices. I. Defect-related and intrinsic breakdown. *Philips J. Res.* **40**, 115–137.

Wolters, D. R. & van der Schoot J. J. 1985*c* Dielectric breakdown in MOS devices. II. Conditions for intrinsic breakdown. *Philips J. Res.* **40**, 137–163.

Wolters, D. R. & van der Schoot, J. J. 1985*d* Dielectric breakdown in MOS devices. III. The damage leading to breakdown. *Philips J. Res.* **40**, 163–185.

Wolters, D. R. & Verweij, J. F. 1986*a* In *Instabilities in silicon devices* (ed. C. Barbottin & A. Vapaille), pp. 315–362. Amsterdam: North Holland.

Wolters, D. R. & van der Schoot, J. J. 1986*b* In *Insulating films on semiconductors* (ed. J. J. Simonne & J. Buxo), pp. 145–149. Amsterdam: North Holland.

Wolters, D. R. & Peek, H. L. 1987*a* Fowler–Nordheim tunneling in implanted MOS Devices. *Solid State Electron.* **30**, 835–539.

Wolters, D. R. & Zegers-van Duijnhoven, A. T. A. 1987*b* Electronic charge transport in thin SiO_2 films. *Appl. Surf. Sci.* **31**, 391–409.

Wolters, D. R. & Zegers-van Duijnhoven, A. T. A. 1989 Trapping of hot electrons. *Appl. Surf. Science* **39**, 565–577.

Xu, M., Tan, C., He, Y. & Wang, Y. 1995 Influence of Fowler–Nordheim tunneling current on the strong inversion high frequency capacitance of thin insulator N-type metal-oxide-semiconductor structures. *Electron. Lett.* **31**, 681–683.

Yoneda, K., Okuma, K., Hagiwara, K. & Todokoro, Y. 1995 The reliability evaluation of thin silicon dioxide using the stepped current Tddb technique. *J. Elect. Chem. Soc.* **142**, 596–600.

Zafar, S., Conrad, K. A., Liu, Q., Irene, E. A., Hames, G., Kuehn, R. & Wortman, J. J. 1995 Thickness and effective electron mass measurements for thin silicon dioxide films using tunneling current oscillations. *Appl. Phys. Lett* **67**, 1031–1033.

Zhang, J. F, Taylor, S. & Eccleston, W. 1992 A quantitative investigation of electron detrapping in SiO_2 under Fowler–Nordheim stress. *J. Appl. Phys.* **71**, 5989–5996.

PHILOSOPHICAL TRANSACTIONS OF THE ROYAL SOCIETY A MATHEMATICAL, PHYSICAL & ENGINEERING SCIENCES

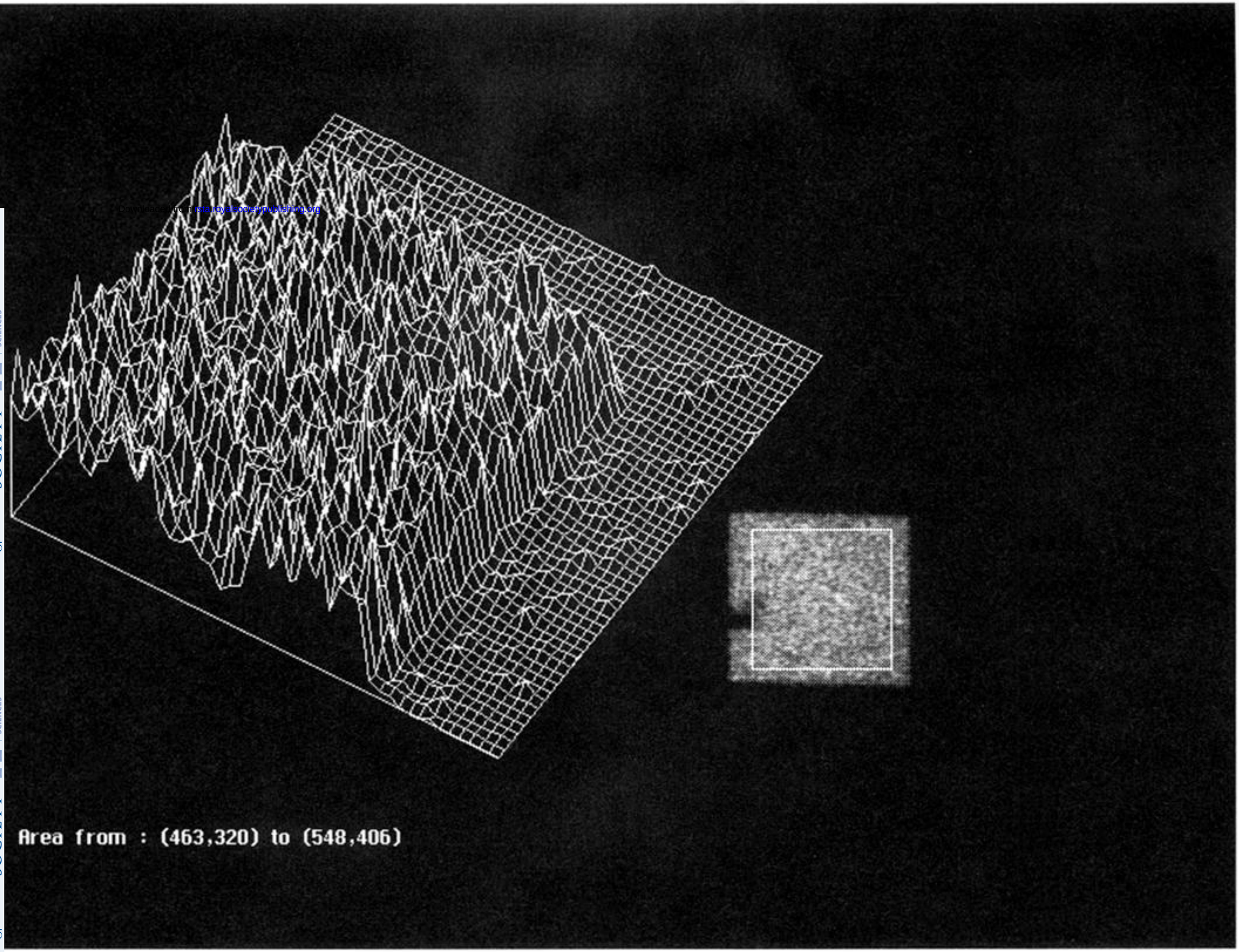

Figure 9. Spatial distribution of photon emission by Fowler–Nordheim currents.

PHILOSOPHICAL TRANSACTIONS OF THE ROYAL SOCIETY A MATHEMATICAL, PHYSICAL & ENGINEERING SCIENCES

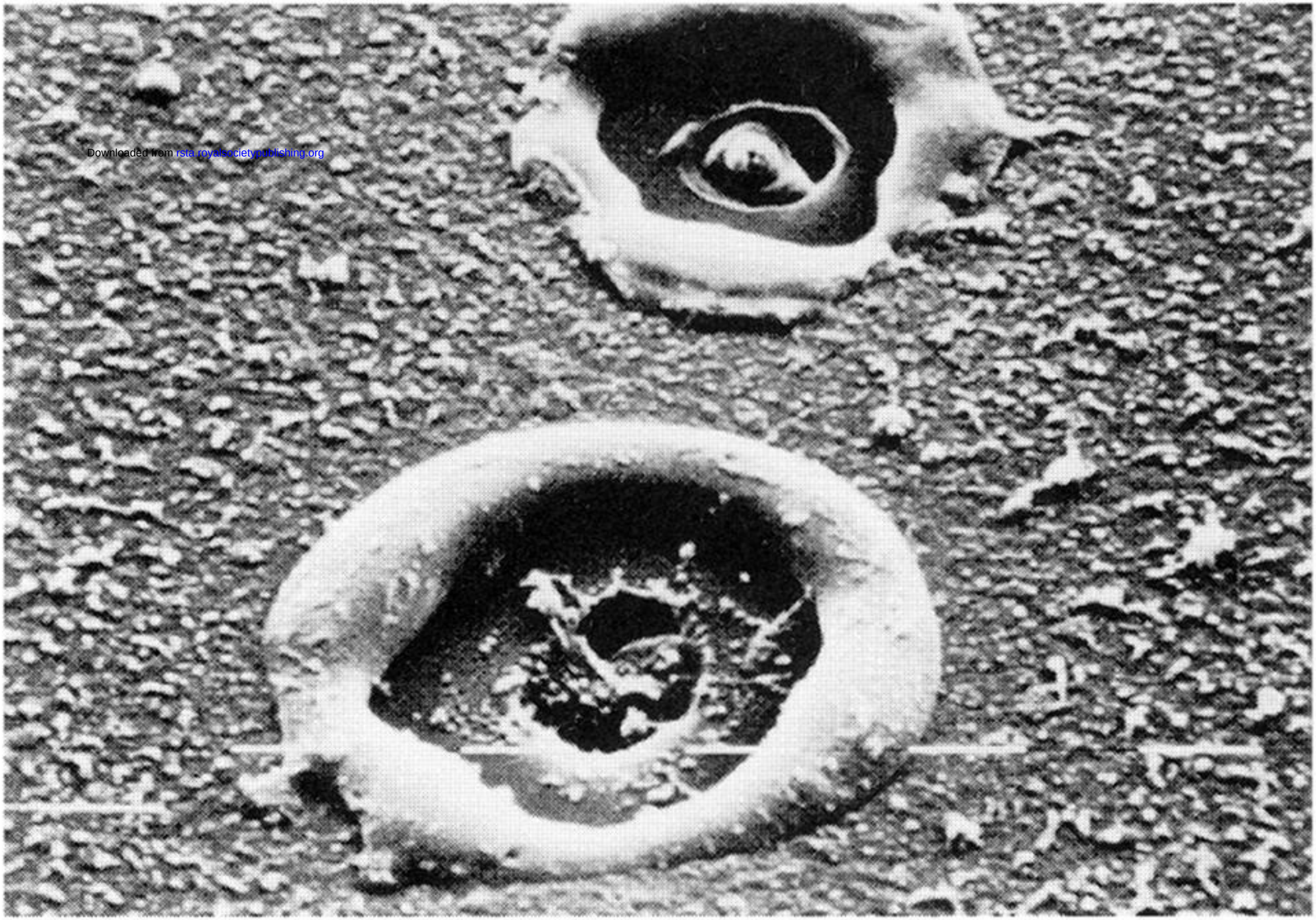

gure 18. The final breakdown of a capacitor leaves a crater, whose dimensions can be calculated om the energy, $\frac{1}{2}CV^2$, stored in the capacitor just before breakdown. There are two craters ecause the first breakdown was self-healing, i.e. the shorting path has been removed by the eakdown. White bars correspond to a length of 1 μm.

PHILOSOPHICAL TRANSACTIONS OF THE ROYAL SOCIETY A MATHEMATICAL, PHYSICAL & ENGINEERING SCIENCES